Available online at www.sciencedirect.com
SCIENCE DIRECT®
Advances in Space Research 33 (2004) 963–969
ADVANCES IN SPACE RESEARCH (a COSPAR publication)
www.elsevier.com/locate/asr

Ionospheric plasma temperatures during 1976–2001 over Millstone Hill

Shun-Rong Zhang *, John M. Holt

MIT Haystack Observatory, Route 40, Westford, MA 01886, USA

Received 26 November 2002; received in revised form 23 June 2003; accepted 9 July 2003

Abstract

Incoherent scatter measurements have been made since the 1960s over Millstone Hill. Zenith antenna data since 1976 and steerable antenna data since 1980 are now available through the WWW-based Madrigal database system. By analyzing this large volume of data in a systematic way, this paper provides an updated climatology of the ionospheric temperature over Millstone Hill, including diurnal variations, solar activity dependences, and the electron density N_e and electron temperature T_e relationship. The daytime T_e in the F2-layer is found to increase with the increasing solar activity in summer, and to decrease in winter. The inverse correlation between N_e and T_e prevails in winter and equinox but is much less pronounced or even disappears in summer. Based on the database, Millstone Hill incoherent scatter radar models are established, and compared with the latest International Reference Model.

Keywords: Ionosphere; Ionospheric temperature; Millstone Hill; Incoherent scatter

1. Introduction

The lack of thermal equilibrium in the earth's upper atmosphere between neutrals, ions, and electrons was suspected by many early researchers. Overwhelming evidences became available in the 1960s from rigorous theoretical calculations, as well as in situ experiments and ground based incoherent scatter experiments which initiated a new era of ionosphere sounding. Based on data collected since that time, researchers have come to a general understanding of the electron temperature (T_e) and ion temperature (T_i) behavior in terms of altitude, local time and latitude variations, as reviewed by, e.g., Schunk and Nagy (1978). Of particular interest in these variations and phenomena have been the predawn enhancement (Carlson and Weill, 1966; Evans, 1967), morning and afternoon maximums (Brace and Theis, 1981), unusually higher night time T_e in winter than in summer above the F peak (Evans, 1973), T_e night time enhancement in winter (Richards et al., 2000), T_e anisotropy (Demars and Schunk, 1987; Oyama and Schlegel, 1988), the electron density (N_e) and T_e correlation (Bilitza, 1975; Mahajan, 1977; Brace and Theis, 1978), features of the topside T_e at low latitudes (Oyama et al., 1997; Balan et al., 1997), etc.

With more and more data becoming available from ground and space, the climatological behavior has been extensively studied to gain a comprehensive view of seasonal, solar cycle, and global variation features (Evans, 1973; Mahajan and Pandey, 1980; Brace et al., 1982; Bilitza and Hoegy, 1990; Otsuka et al., 1998). Recent research interests in ionospheric plasma temperatures have turned significantly to the data modeling and model-data comparison. These include the modeling of in situ measurements from AEROS-A (Spenner and Plugge, 1979), from AE-C, ISIS-1 and ISIS-2 (Brace and Theis, 1981), and recently from the Intercosmos satellites (Truhlik et al., 2000), each of the three models being incorporated into the International Reference (IRI) model (Bilitza et al., 1985; Bilitza, 2001). Titheridge (1998) developed a plasma temperature model to represent variations with altitude along a magnetic field

* Corresponding author. Tel.: +1-781-981-5725; fax: +1-781-981-5766.
E-mail address: shunrong@haystack.nit.edu (S.-R. Zhang).

0273-1177/$30 © 2003 COSPAR. Published by Elsevier Ltd. All rights reserved.
doi:10.1016/j.asr.2003.07.012

line. Buonsanto (1989) made comparisons between the IRI model and a number of individual temperature measurements from the Millstone Hill incoherent scatter (IS) radar.

The Millstone Hill radar (MHR) provides reliable ionospheric temperature data that were first published by Evans (1962). Over the ensuing 40 years, hundreds of scientific papers and technical reports have well determined a variety of features in the mid-latitude and sub-auroral ionosphere. Previous publications, however, dealt mostly with individual observations or with data for a few years at most, and since the late 1970s, there have been few publications on ionospheric temperature profiles, although a large quantity of additional data has been collected. It is very important that we revisit the early accomplishments making use of the much larger data set now available. Recently, a robust WWW-based database system, Madrigal (http://www.openmadrigal.org), has been established to handle distributed data management and distribution for large upper atmospheric facilities, including MHR, across the world. MHR data from 1970 onward are now available online; this makes it feasible in an efficient and systematic way to conduct climatology studies and data modeling. Based on this huge database, this paper will provide an updated climatology of ionospheric temperatures over Millstone Hill. We will discuss some of the typical variations shown in the data and examine the N_e–T_e correlation, We will also present the Millstone plasma temperature model, and compare it with the IRI model.

2. Ionospheric temperature climatology over Millstone Hill

The Millstone Hill UHF IS radar system operates with a zenith-directed 68-m diameter fixed parabolic antenna, which commenced operation in 1963, and a fully-steerable 46-m antenna, which commenced operation in 1978. Radio signals are transmitted at 440 MHz by two 2.5-MW transmitters. For various experiment modes, different pulse lengths, coded or uncoded, are transmitted giving different temporal and spatial resolutions. The IS experiments are carried out for more than 1000 h per year, totaling 960 observation periods by the end of 2001.

In this study, we concentrate on data above Millstone Hill within 5° latitude of the radar (local measurements), and we consider data from quiet magnetic conditions when 3-h ap index < 10; we leave discussions on magnetic effects to a future paper. To separate various obvious effects, we bin data according to altitude, solar local time and month; to demonstrate the solar activity dependence, we also sort data according to the daily solar 10.7 cm flux index F107.

2.1. Diurnal and seasonal changes

In summer, T_e variations exhibit the simplest pattern: for diurnal variations, a large increase after sunrise is followed by a period when T_e remains almost constant, and by sunset T_e decreases slowly. The nocturnal T_e is much lower than the daytime one. T_e increases essentially monotonically with altitude. The increase at high altitude is an indication of plasmaspheric heat source for the ionosphere.

T_e variations in winter are much more complicated (Fig. 1(a)). The most striking feature is the morning enhancement which develops above 200 km and is much stronger during high solar activity. Compared to low solar activity, the level of daytime T_e is very low at high solar activity, yielding a diurnal variation of small amplitude, due to the larger electron density at high solar activity (Fig. 1(b)). During the winter night, since the conjugating ionosphere is still sunlit, photoelectrons may reach the ionosphere above Millstone and prevent T_e from decreasing rapidly. On the other hand, as electron density decays and electron cooling decreases, T_e tends to increase. Then after midnight, the winter N_e enhancement that peaks around 3LT (see Fig. 1(b)) leads to decrease in T_e.

At low levels of N_e (low solar activity), T_e increases with altitude monotonically (Fig. 2(a)). At high levels of N_e, a low temperature region is formed on the T_e altitude profile. The minimum is about 20–30 km above the F2 peak (Fig. 2(b)). A local electron density $N_e > \sim 10^{12}$ m^{-3} appears to be a necessary condition for the development of temperature minimum (Evans, 1971; also see Fig. 2(b)). We will further discuss the N_e and T_e relationship later.

Fig. 2(a) gives also T_i profiles to demonstrate the difference between T_e and T_i. The ion thermal balance is straightforward for mid-latitudes. At low altitudes, coupling of ions to the colder neutrals dominates that to the hotter electrons and T_i equals the neutral temperature T_n. At higher altitudes, coupling to the hotter electrons dominates but coupling to the neutrals is still significant and $T_e > T_i > T_n$.

2.2. Solar activity dependence

The solar EUV flux affects the electron temperature through several mechanisms. An enhanced flux gives rise to more photoelectrons which in turn elevate plasma temperatures by heating processes. Meanwhile, the increased electron density leads to an enhanced electron cooling rate, which may lead to lower T_e. The actual response of T_e to a change in solar EUV is the result of the two competing processes. In summer when the level of N_e is low, a larger EUV flux results in a higher T_e because the heating rate increases more than the cooling rate; in winter when N_e is high, a larger EUV flux results

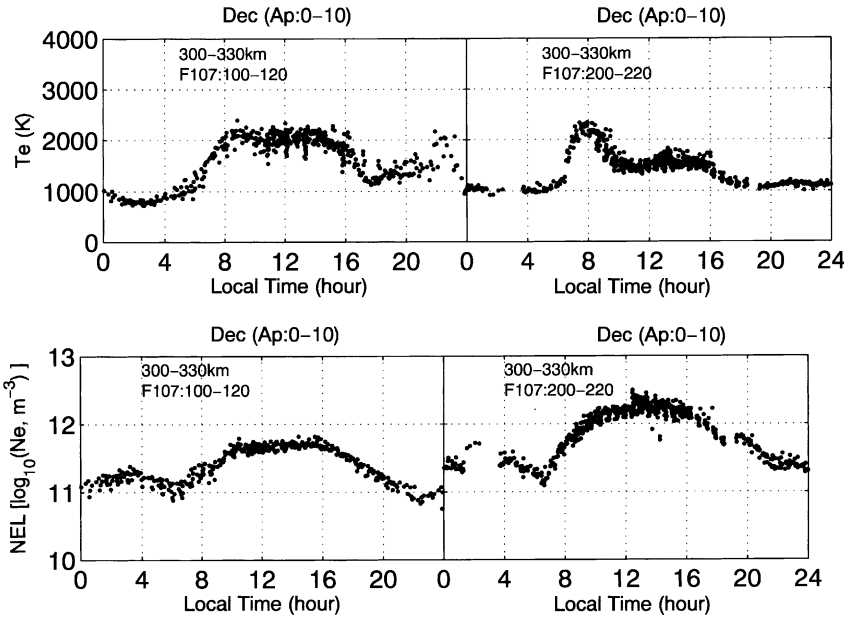

Fig. 1. Diurnal variations of T_e (a, upper panels), and N_e (b, bottom panels) in December for the height range 300–330 km at low (left panels) and high (right panels) solar activities. Points shown in the plots are all data meeting the month, altitude, F107 and Ap criteria.

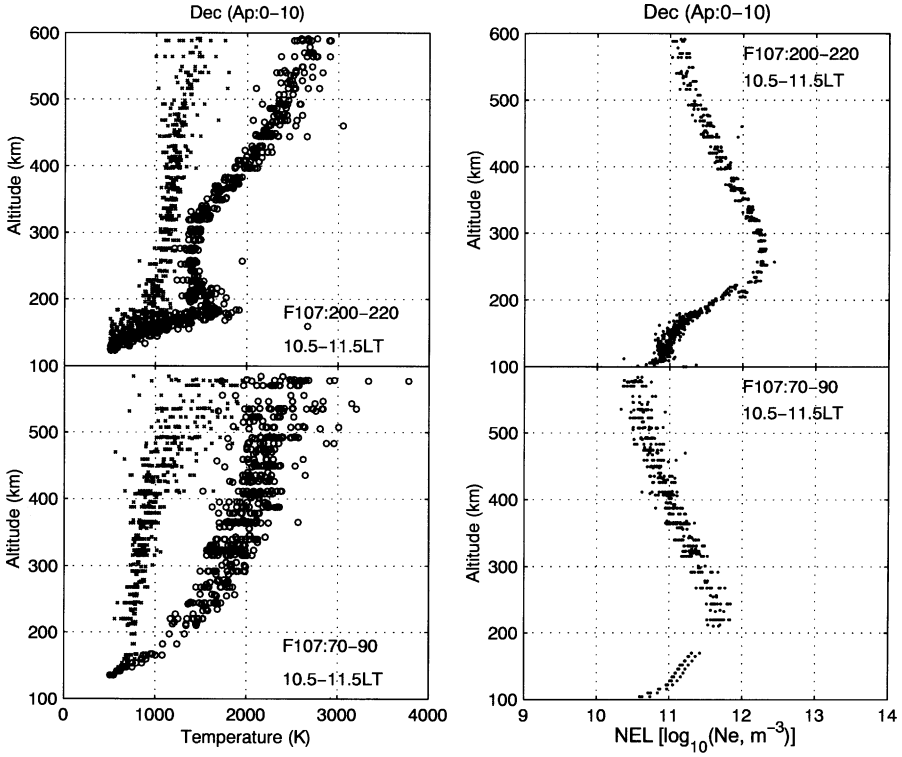

Fig. 2. Profiles of plasma temperatures (a, left panels) and electron density (b, right panels) for December between local time 1030–1130 for high (upper panels) and low (bottom panels) solar activities. (Open circles are T_e and crosses are T_i.) Points shown in the plots are all data meeting the month, local time, F107 and Ap criteria.

in a lower T_e. This is demonstrated in Fig. 3(a) which plots seasonal variations of the gradient $dT_e/dF107$ at 14 LT for altitudes 300 and 400 km. The gradient is the slope of the straight line for linear regression of the T_e data points to the corresponding F107 values. As for the diurnal variation (Fig. 3(b)), the gradient in winter turns

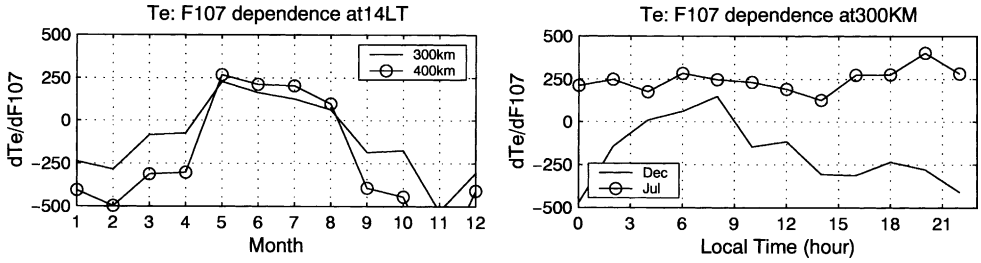

Fig. 3. Variations of the gradient $dT_e/dF107$, defined as the slope of the straight line for linear regression of T_e to the normalized F107, (F107-135)/100, as a function of month (a, left panel) at 1400LT, and as a function of local time (b, right panel) at 300 km.

to be positive in the morning when the heating is increasing more rapidly than N_e so that the heating dominates the energy balance.

As the solar activity increases, T_i increases at low altitudes following the corresponding neutral T_n changes, and at high altitudes due to increased energy transport from electrons.

2.3. N_e–T_e interrelationship

We have mentioned the T_e–N_e relationship in the previous discussions. The energy balance equation for electrons can be simplified as follows,

$$\sin^2 I \frac{\partial}{\partial h}\left(K^e \frac{\partial T_e}{\partial h}\right) + \sum Q_e - \sum L_e = 0, \quad (1)$$

where the first term on the left side is heat conduction, which becomes important above 300 km, the second term is electron heating, which is due to photoelectrons at low altitudes, and by Coulomb interactions with ions at high altitudes, and the third term is the cooling rate. The electron cooling is proportional to N_e, thereby tending to yield an inverse correlation between T_e and N_e. However, a large N_e often means a large rate of ionization, resulting in the generation of more photoelectrons which lose their energy to ambient electrons through elastic collisions and to neutrals through inelastic collisions. Fig. 4(a) shows a very well defined inverse relationship between N_e and T_e during the day in December. Here, a linear function of $\log N_e$ may be used to represent the T_e changes (Bilitza, 1975). This relationship is remarkably pronounced in winter and equinox seasons above 250 km. In summer, however, it changes substantially with time and altitude, and may become positive in some circumstances. Fig. 4(b) shows some of the summer results.

In fact, as shown in Fig. 5(a) which gives contours of the linear correlation coefficient between T_e and N_e vs altitude and local time for July, a positive correlation prevails in summer during almost the entire day in the F2 region. In March (Fig. 5(b)), however, except for sunrise and sunset-evening periods, the inverse correlation is well defined above the F2 peak.

3. Millstone model and IRI comparisons

Based on all the local measurements, MHR models for N_e, T_e, T_i and parallel drifts V_0 have been created (Holt et al., 2002). This version of the models presented here takes into account all E and F region data since 1970 between 100 and 1000 km altitude. To achieve a high seasonal resolution, we separate the data into 12 months; we further bin the data into hourly local time bins and model the altitude variation by a piecewise linear function with nodes at 100, 110, 120, 130, 140,

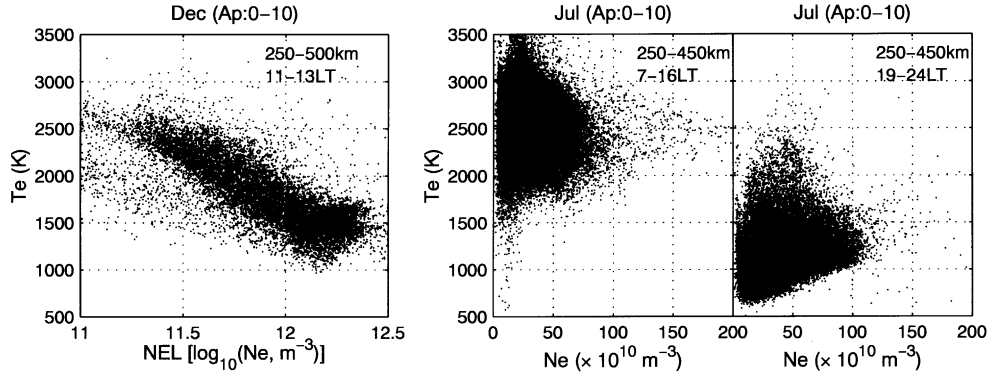

Fig. 4. Scatter plots of T_e and N_e relationship for December (a, left panel), and for summer (b, middle and right panels) during the day and during the night.

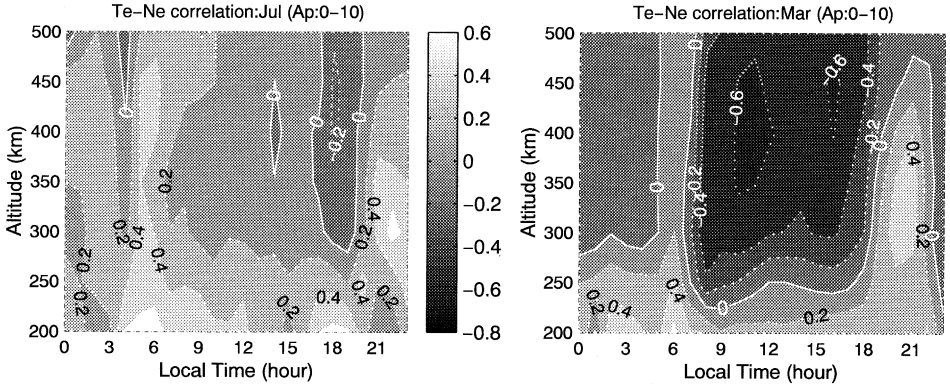

Fig. 5. T_e–N_e correlation coefficient contours for July (a, left panel) and March (b, right panel).

160, 180, 200, 225, 250, 300, 400, 500, 600, 700 and 1000 km. Then a least-square-fit is performed to determine the altitude, solar activity and magnetic activity dependences using F107 index for the previous day and ap index for the previous 3 h, i.e., $P = \beta_0 + \beta_1 \times (F107-135)/100 + \beta_2 \times (ap-15)/10$, where P is either N_e, T_e, T_i, or V_0. Fitting coefficients β are obtained for each bin.

These MHR models are compared with IRI values for three days (day 90, 210 and 330) representing equinox, summer and winter at the level of high solar activity (F107 = 200). We use the latest IRI2000 model with its standard model options, except for T_e. T_e is calculated with IRI using the option of Truhlik et al. (2000) Intercosmos satellite based T_e model. This model is expected to give better results for high solar activity at

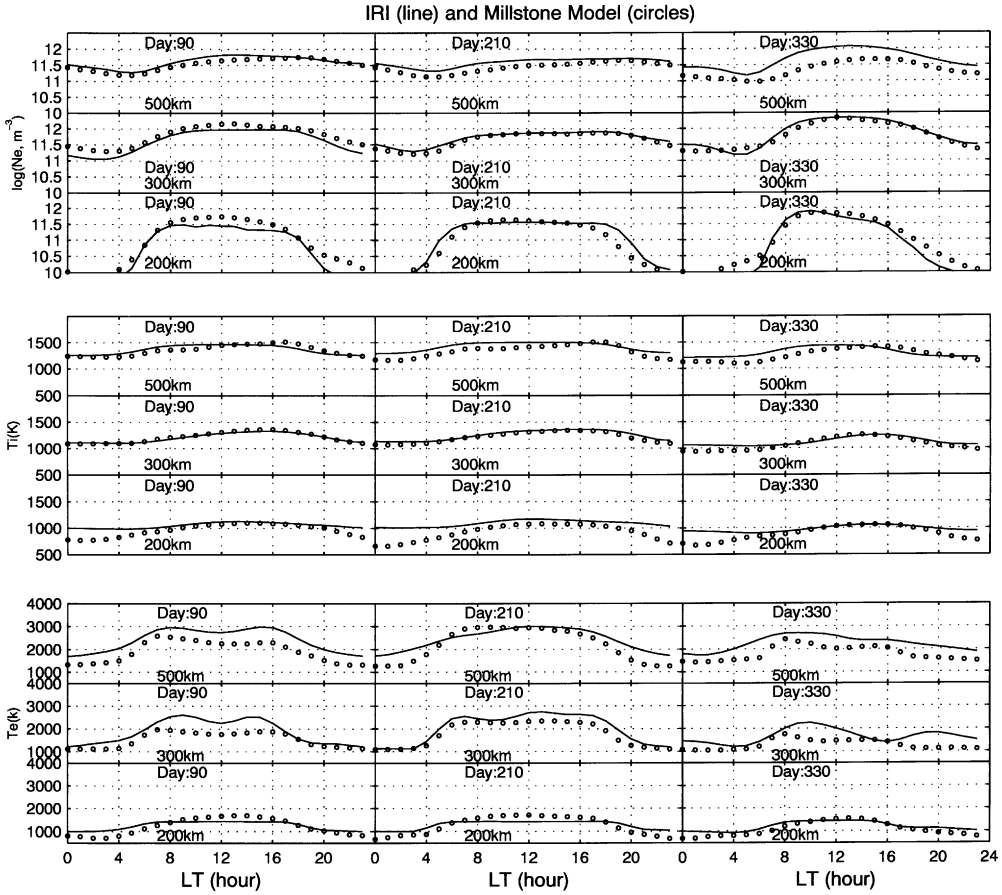

Fig. 6. Millstone model and IRI comparisons for N_e (a, upper middle panels), T_i (b, left panels) and T_e (c, right panels) for F107 = 200 on the day numbers 90 (spring), 210 (summer) and 330 (winter) at various altitudes over Millstone.

altitudes above 500 km. The top three panels in Fig. 6 show the electron density comparisons. Excellent agreement can be seen for F region heights, except that IRI overestimates topside N_e in winter. The overestimate agrees with results of other studies based on the in situ topside sounding. Ion temperatures (middle panels) show agreement at 300 km and above. At lower altitudes, the IRI temperature, largely based on a model neutral temperature, is higher by night than the observed one. As for T_e (bottom panels), the IRI model at 500 km is characterized by an overshoot in the morning which does not occur in summer over Millstone (and does not in the MU radar site as well, see Otsuka et al., 1998). Around the F2 peak height, agreement is achieved in summer, and for other seasons IRI overestimates the measured Millstone Hill values during the day.

4. Concluding remarks

By systematically analyzing incoherent scatter data taken from 1970 to the present, this paper provides an updated climatology of ionospheric thermal behavior over Millstone Hill. We have discussed the diurnal variation and solar activity dependence, and examined the electron density N_e and electron temperature T_e relationship. It is indicated that T_e in the F2-layer during the day increases with the level of solar activity in summer, but decreases in winter, mainly due to the changing relative importance of the cooling in association with seasonal changes in N_e. The inverse correlation between N_e and T_e prevails in winter and equinox essentially during the day, but is much less pronounced or even disappears in summer.

Based on data collected over more than 30 years, Millstone Hill incoherent scatter radar models have been established. Comparisons between the models and the International Reference Model indicate good agreements in electron density, except in winter when IRI N_e tends to be higher at topside. The latest IRI overestimates the daytime electron temperature at the F2 peak height in equinox and winter, and yields a higher nighttime ion temperature at 200 km.

Acknowledgements

We thank the members of the Haystack Observatory Atmospheric Sciences Group for assembling and maintaining the Madrigal Database of Millstone Hill incoherent scatter radar observations, which were the basis of this study. This research was supported by NSF Space Weather Grant ATM-0207748. The Millstone Hill incoherent scatter radar is supported by a cooperative agreement between the National Science Foundation and the Massachusetts Institute of Technology. We thank Dr. D. Bilitza for making the IRI model codes available to us.

References

Balan, N., Oyama, K.-I., Bailey, G.J., Fukao, S., Watananabe, S., Abdu, M.A. A plasma temperature anomaly in the equatorial topside ionosphere. J. Geophys. Res. 102, 7485, 1997.

Bilitza, D. Models for the relationship between electron density and temperature in the upper ionosphere. J. Atmos. Terr. Phys. 37, 1219–1222, 1975.

Bilitza, D. International Reference Ionosphere 2000. Radio Sci. 36, 261–275, 2001.

Bilitza, D., Brace, L., Theis, R. Modelling of ionospheric temperature profiles. Adv. Space Res. 5 (7), 53–58, 1985.

Bilitza, D., Hoegy, W.R. Solar activity variations of ionospheric plasma temperatures. Adv. Space Res. 10 (8), 81–90, 1990.

Brace, L.H., Theis, R.F. An empirical model of the interrelationship of electron temperature and density in the daytime thermosphere at solar minimum. Geophys. Res. Lett. 5, 275–278, 1978.

Brace, L.H., Theis, R.F. Global empirical models of ionospheric electron temperature in the upper F-region and plasmasphere based on in situ measurements from the Atmosphere Explorer-C, ISIS-1 and ISIS-2 Satellites. J. Atmos. Terr. Phys. 43, 1317–1347, 1981.

Brace, L.H., Theis, R.F., Hoegy, W.R. A global view of F-region electron density and temperature at solar maximum. Geophys. Res. Lett. 9, 4883–4886, 1982.

Buonsanto, M.J. Comparison of incoherent scatter observations of electron density, and electron and ion temperature at Millstone Hill with the International Reference Ionosphere. J. Atmos. Terr. Phys. 51, 441–468, 1989.

Carlson, H.C., Weill, G.M. Ionospheric heating by magnetic conjugate point photoelectrons. J. Geophys. Res. 71, 195–199, 1966.

Demars, H.G., Schunk, R.W. Temperature anisotropies in the terrestrial ionosphere and plasmasphere. Rev. Geophys. 25, 1659–1679, 1987.

Evans, J.V. Diurnal variation of the temperature of the F region. J. Geophys. Res. 67, 4914, 1962.

Evans, J.V. Midlatitude electron and ion temperatures at sunspot minimum. Planet. Space Sci. 15, 1557–1570, 1967.

Evans, J.V., Millstone Hill Thomson scatter results for 1967 Technical Report 482, Lincoln Laboratory, MIT, 22 July 1971.

Evans, J.V. Seasonal and sunspot cycle variation of F region electron temperatures and protonospheric heat flux. J. Geophys. Res. 78, 2344–2349, 1973.

Holt, J.M., Zhang, S.-R., Buonsanto, M.J. 2002. Regional and Local Ionospheric Models Based on Millstone Hill Incoherent Scatter Radar Data, Geophys. Res. Lett., 29, 0.1029/2001GL013579, 2002.

Mahajan, K.K. Models of electron temperature in the ionospheric F-region using electron density height profiles. J. Atmos. Terr. Phys. 39, 637–639, 1977.

Mahajan, K.K., Pandey, V.K. Models of electron temperature in the topside ionosphere for low and medium solar activity conditions. J. Geophys. Res. 85, 213–216, 1980.

Otsuka, Y., Kawamura, S., Balan, N., Fukao, S., Bailey, G.J. Plasma temperature variations in the ionosphere over the middle and upper atmosphere radar. J. Geophys. Res. 103, 20, 705-20, 713, 1998.

Oyama, K.I, Schlegel, K. Observations of electron temperature anisotropy in the ionosphere: a review. Ann. Geophys. 6, 389, 1988.

Oyama, K.-I., Abdu, M.A., Balan, N., Bailey, G.J., Watanabe, S., Takahashi, T., de Paula, E.R., Batista, I.S., Isoda, F., Oya, H. High electron temperature associated with the prereversal enhancement in the equatorial ionosphere. J. Geophys. Res. 102, 417, 1997.

Richards, P.G., Buonsanto, M.J., Reinisch, B.W., Holt, J., Fennelly, J.A., Scali, J.L., Comfort, R.H., Germany, G.A., Spann, J., Brittnacher, M., Fok, M.-C. On the relative importance of convection and temperature to the behavior of the ionosphere in North America during January 6–12, 1997. J. Geophys. Res. 105 (12), 763–767, 2000.

Schunk, R.W., Nagy, A.F. Electron temperatures in the F region ionosphere: theory and observations. Rev. Geophys. Space Phys. 16, 355–399, 1978.

Spenner, E., Plugge, R. Empirical model of global electron temperature distribution between 300 and 700 km based on data from AEROS-A. J. Geophys. Res. 46, 43–56, 1979.

Titheridge, J.E. Temperatures in the upper atmosphere and plasmasphere. J. Geophys. Res. 103, 2261–2277, 1998.

Truhlik, V., Triskova, L., Smilauer, J., Afonin, V. Global empirical model of electron temperatures in the outer ionosphere for period of high solar activity based on data of Intercosmos satellites. Adv. Space Res. 25 (1), 163–172, 2000.